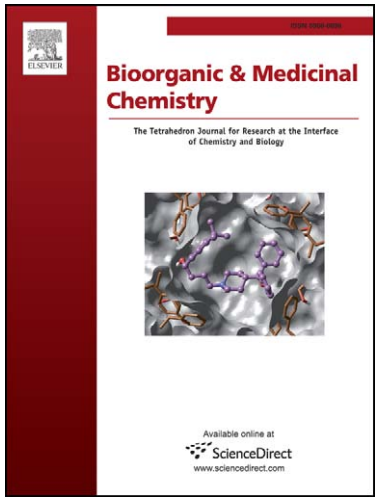

Screening of herbal constituents for aromatase inhibitory activity

S. Paoletta, G.B. Steventon, D. Wildeboer, T.M. Ehrman, P.J. Hylands, D.J. Barlow

PII: S0968-0896(08)00758-X
DOI: 10.1016/j.bmc.2008.08.034
Reference: BMC 6814

To appear in: *Bioorganic & Medicinal Chemistry*

Received Date: 29 April 2008
Revised Date: 5 August 2008
Accepted Date: 13 August 2008

Please cite this article as: S. Paoletta, G.B. Steventon, D. Wildeboer, T.M. Ehrman, P.J. Hylands, D.J. Barlow, Screening of herbal constituents for aromatase inhibitory activity, *Bioorganic & Medicinal Chemistry* (2008), doi: 10.1016/j.bmc.2008.08.034

Screening of herbal constituents for aromatase inhibitory activity

S. Paoletta, G.B. Steventon, D. Wildeboer, T.M. Ehrman, P.J. Hylands, D.J. Barlow*

Pharmaceutical Science Division, King's College London, Franklin Wilkins Building, 150 Stamford Street, London SE1 9NH

*Author for correspondence: D.J. Barlow
Telephone: +44 (0) 207 848 4827
e-mail: dave.barlow@kcl.ac.uk

Random Forest screening of the phytochemical constituents of 240 herbs used in traditional Chinese medicine identified a number of compounds as potential inhibitors of the human aromatase enzyme (CYP19). Molecular modelling/docking studies indicated that three of these compounds (myricetin, liquiritigenin and gossypetin) would be likely to form stable complexes with the enzyme. The results of the virtual screening studies were subsequently confirmed experimentally, by *in-vitro* (fluorimetric) assay of the compounds' inhibitory activity. The IC-50s for the flavones, myricetin and gossypetin were determined as 10 μM and 11 μM, respectively, whilst the flavanone, liquiritigenin, gave an IC-50 of 0.34 μM – showing about a 10 fold increase in potency, therefore, over the first generation aromatase inhibitor, aminoglutethimide.

Keywords

Cytochrome P450, CYP19, aromatase, traditional Chinese medicine, myricetin, gossypetin, liquiritigenin

Introduction

Around one-in-nine women in the UK are diagnosed with breast cancer at some point in their life [1], and 50-80% of these suffer tumours that are oestrogen-dependent [2] – with the tumour cells expressing oestrogen receptors, and the growth of the tumours being stimulated by circulating oestrogen. These oestrogen-dependent mammary carcinomas can be combated through the use of anti-oestrogens (like tamoxifen), that interfere with the binding of oestrogen to its receptor, or else through the use of aromatase inhibitors, that act to decrease the circulating levels of oestrogen by blocking the biosynthesis of the compound from androgens [3].

Aromatase, also known as CYP19, is produced to high levels in breast tissue, and particularly in those areas in and around tumour sites [3]. The enzyme is competitively inhibited by steroidal compounds like exemastane, but also by various non-steroidal compounds, such as aminoglutethimide (Figure 1). The orally-active, potent, and highly selective (third generation) aromatase inhibitors that are licensed for clinical use (in the treatment of metastatic oestrogen-dependent breast cancer in postmenopausal women) include anastrozole, letrosole and exemastane (Figure 1).

Other known inhibitors of the enzyme include various flavonoid compounds, in particular those based on the flavone and flavanone skeletons [3]. These compounds have attracted considerable interest in regard to aromatase inhibition, in part because of the hypothesis put forward that these natural products may represent dietary factors that account for the significantly lower incidence of breast cancer among women of Asian and Oriental origin [4], and also because of the reported general inverse association between the incidence of breast cancer and consumption of flavonoid-rich vegetables [5-6].

In the work reported here, the aim was to use the structural data on the phytochemical constituents from herbs commonly used in traditional Chinese medicines, to prospect for novel aromatase inhibitors, using a combination of multiple decision tree (Random Forest) modelling and molecular docking studies, with the hits identified through these *in-silico* predictions then confirmed through laboratory-based experiments.

Methods

Random Forest Modelling Structural data on the known phytochemical constituents of 240 herbs widely used in traditional Chinese medicine were taken from the Chinese Herbal Constituents Database (CHCD) [7]. A total of 238 different structural descriptors for these compounds were then computed; specifically, the full set of 150 2D MOE descriptors (Chemical Computing Group, Montreal, Quebec), 56 Kier-Hall descriptors [8-9], and 32 Labute VSA descriptors [10]. Random Forest (RF) models for prediction of aromatase inhibitory activity were derived using activity data taken from the Bio-active Plant Compounds Database (BPCD) [7]. The RF modelling, performed using *Random Forests, version 1* (Salford Systems, San Diego, California) was carried out as described by Ehrman *et al* [11-12]. The MOE, Kier-Hall and Labute descriptor sets were used in generating three separate RF models, each comprising an ensemble of 500 decision trees. For each tree in the ensemble, a bootstrap sample was randomly chosen from the minority class of 44 BPCD compounds with known anti-aromatase activity, and the same number of cases then randomly selected to add to this group from the majority class of 8,264 CHCD compounds. Decision trees were then constructed, following the CART algorithm, and employing the Gini splitting criterion (see [11-12]). The error rates associated with the resulting RF predictions were quantified using the technique of "out-of-bag" (OOB) cross-validation, with ~33% of the bootstrap compounds withheld for each tree trained in order to provide an independent test sample. By such means the prediction performance of the RF is measured by taking the OOB sample for each tree, running it through that tree, computing the associated error rate, and then averaging the error rates over all 500 trees to obtain the mean misclassification rate for the entire forest. The mean misclassification rates thus obtained (calculated with an RF cut-off value of 0.5) were 30%, 21%, and 32%, for the RF models generated using the MOE, Kier-Hall and Labute descriptor sets, respectively. In the present work, however, much more stringent criteria were employed to identify potential aromatase inhibitors: the CHCD compounds taken as hits being those that achieved aromatase activity RF scores of ≥ 0.8 in at least two of the three RF models (a score of 0.8 here meaning that 80% of the decision trees within a given RF model voted for a compound to exhibit aromatase activity). By such means the resulting predictions were made more dependable, but with the attendant limitation that the CHCD hits would then be (structurally) very similar to the bioactive compounds most numerous in the RF training set, *viz.*, the flavonoids.

Molecular Modelling The construction of molecular models of potential aromatase inhibitors, and the docking of these ligands into the enzyme active site, were first performed using Hyperchem™ version 7 (Hypercube Inc., Gainesville, Florida). The atomic co-ordinates for the homology modelled structure of human aromatase were downloaded from the Protein Data Bank [13] (accession code, 1TQA, [14]). Ligands were initially docked manually, and the resulting complexes then optimised using the AMBER force field [15], with Polak-Ribière conjugate gradient minimisation to a final potential energy gradient of 0.001 kcal.mole^{-1}.Å^{-1}. For each of the three ligands, a total of five initial poses were considered (with superposed centroids but varying orientations), and the optimisation of these complexes performed with movement allowed only to the ligand atoms (all protein atoms being treated as fixed). Further docking studies were subsequently performed using the FlexX program [16] (BioSolveIT GmbH, Sankt Augustin, Germany). In this case, the protein residues involved in the binding site for each ligand were defined with reference to the ligand pose in the most stable of the Hyperchem™-modelled complexes. The FlexX docking was in all cases performed without constraints, and using the default values for all adjustable control parameters.

In-vitro assay of aromatase inhibitory activity Liquiritigenin (7-hydroxy-2-(4-hydroxyphenyl)chroman-4-one), gossypetin (2-(3,4-dihydroxyphenyl)-3,5,7,8-tetrahydroxychromen-4-one) and myricetin (3,5,7-trihydroxy-2-(3,4,5-trihydroxyphenyl)chromen-4-one) were purchased from LGC Standards Ltd (Teddington, UK) and were used as received. Aromatase inhibition assays were performed using the CYP19/MFC high-throughput screening kit (BD Biosciences, Oxford, UK). Substrate for the reaction was 7-methoxy-4-trifluoromethyl coumarin (MFC). Enzyme reactions were performed, according to the manufacturer's protocol, using ethanol solutions of the potential inhibitors, in Greiner (flat bottom, black) 96-well plates (Sigma, Dorset, UK), with fluorescence measurements recorded using a FLUOstar Optima (BMG Labtech Ltd, Aylesbury, UK), and employing an excitation wavelength of 405 nm and emission wavelength of 520 nm. All assays were performed at ambient, and fluorescence measurements recorded at five-minute intervals over a period of 1 hr. A CYP19 concentration of 7.5 nM was employed, with a fixed substrate concentration of 25 μM. Fluorescence-time profiles for each reaction were corrected for background fluorescence, and the initial catalytic rates in the presence of inhibitor expressed as a fraction of the rate for the uninhibited enzyme. The assays for the TCM constituents were carried out in duplicate on two separate occasions, but the assay for ketoconazole was carried out only in triplicate (on a single occasion).

Results & Discussion

The structural features of 44 phytochemicals with known aromatase activity were used in training Random Forest (RF) models to distinguish likely aromatase inhibitors in 8,264 constituents of 240 different herbs used in traditional Chinese medicine (TCM). The compounds with known aromatase activity comprised eighteen assorted flavonoids (55% of the total), nine sesquiterpenes (27% of the total), with the remainder including alkaloids, tannins, lignans, di- and tri-terpenes, aliphatics and sterols. The trivial names for the 30 TCM compounds achieving the highest RF scores in this screening are listed in Table 1, along with their systematic names, botanical source(s) and anti-aromatase RF scores. Several of the hits identified are for compounds already known to inhibit the aromatase enzyme, including apigenin (with an IC-50 of ~1 μM) [17], and diadzein, genistein, and galangin (with K_i values of the order of 100 μM) [18]. Of the 22 compounds in this short list that do not appear yet to

have been tested for anti-aromatase activity, three compounds, namely, liquiritigenin, gossypetin, and myricetin could be obtained commercially. These compounds (the chemical structures for which are shown in Figure 2) were selected for further study. Myricetin has long been recognised as an anti-oxidant [19] and is also shown to inhibit mitogen-activated protein kinase kinase [20]. Liquiritigenin has been shown to have apoptotic [21] and cytotoxic [22] effects, and also to inhibit tyrosinase [23] and monoamine oxidase [24]. Gossypetin has previously been shown to have anti-inflammatory [25] and anti-allergic [26] activity.

In order to provide a further test of the likely inhibitory activity of the three chosen herbal constituents against human aromatase, *in-silico* experiments were conducted to dock the ligands into the enzyme binding site, both manually and using the FlexX [16] software. For each ligand, various initial poses were considered, but all in the vicinity of residues previously identified (on the basis of the model building studies) as lining the enzyme active site pocket [14]. These residues - many of which have also been demonstrated to be key determinants in ligand binding through site-directed mutagenesis experiments [18, 27-30] – include Glu 302, Thr 310, Ser 478 and His 480.

On the basis of the manual docking, it was shown that the two flavones, gossypetin and myricetin did not give as good a fit to the enzyme binding site as the flavanone, liquiritigenin. For the flavones, the potential energies of the complexes were in the range -88 - -67 kJ.mole^{-1} and -67 - -38 kJ.mole^{-1} (for myricetin and gossypetin, respectively), whereas the energies for the liquiritigenin complexes lay in the range -105 - -84 kJ.mole^{-1}. On the basis of the manual docking, therefore, liquiritigenin was predicted to show a greater inhibitory activity against aromatase than either of the two flavones. Liquiritigenin, with its L-shaped form, dictated by the conformational flexibility of the heterocyclic ring and the α-substituent at C-2, appears better suited to the shape of the enzyme binding site than the more planar flavones (see Figure 3). Although the most stable of the manually docked liquiritigenin complexes showed no protein-ligand hydrogen bonds, such interactions were seen in some of the lower ranked structures, typically between the ring hydroxyls and various sites on the protein main chain.

In the FlexX docking studies, the highest scoring (most stable) complexes were found to be those involving myricetin and gossypetin. The energies for the top 20 poses ranged from -23 to -13 kJ.mole^{-1} for myricetin, and from -20 to -12 kJ.mole^{-1}for gossypetin. In contrast, the top 20 poses for liquiritigenin complexes gave energies in the range -18 to -9 kJ.mole^{-1}. Inspection of the FlexX modelled complexes for the two flavone ligands revealed that the improved binding was often associated with a twisting of the chromene and phenyl rings – with the C2-C1' dihedral angle generally increased from ~0^{o} to ~60^{o} (see Figure 4). Such twisting (which was not seen in any of the Hyperchem™ optimised models) seemed to allow for greater protein-ligand hydrogen bonding.

It was found, therefore, that the FlexX and manual docking studies were not consistent: the latter suggested that the order of anti-aromatase activities would be myricetin > gossypetin > liquiritigenin, whereas the former suggested that the order would be liquiritigenin > myricetin > gossypetin. Laboratory-based assays were thus conducted for all of the compounds.

In-vitro testing of the activities of the putative aromatase inhibitors was carried out by means of a coupled fluorometric assay, monitoring the reduction in fluorescence associated with formation of the CYP19 product (7-hydroxy-4-trifluoromethyl coumarin). IC-50s for each inhibitor, including that for the positive control, ketoconazole, were determined from the percentage inhibition-concentration plots (Figure 5). For the flavones, myricetin and

gossypetin, (Figure 5B,C) the IC-50s were found to be 10 μM and 11 μM, respectively, whereas that for the flavanone, liquiritigenin (Figure 5A) was found to be 0.34 μM. The IC-50 for ketoconazole (Figure 5D) was recorded as 3 μM – consistent with the value of 3.8 μM quoted by the suppliers.

It is seen, therefore, that the rank ordering of the activities for the three TCM compounds agrees with the ordering predicted on the basis of the manual docking studies, but not that predicted on the basis of the FlexX docking studies. In part this might be attributed to the emphasis given by FlexX to establishing hydrogen bonding between the ligands and protein – such that the polyhydroxylated flavones erroneously appear capable of forming more extensive interactions with the aromatase enzyme than the (dihydroxy) flavanone, liquiritigenin. It must also be borne in mind, however, that the agreement between the manual docking and *in-vitro* test results may be entirely fortuitous, since neither the manual docking nor the FlexX docking studies allowed for any conformational changes in the protein, nor did they take into account the associated entropic changes (with the stability of the complexes judged purely in terms of their potential energies). With this in mind then, it is perhaps better simply to record that both the manual docking and FlexX docking studies indicated that all three of the TCM compounds would be likely to form stable complexes with the aromatase enzyme, and that this was borne out in the experimental studies.

Several recent reviews (*cf*. [31-32]) have attested to the benefits to be gained through the application of virtual screening methods in large scale data mining of natural product databases, with much improved levels of success seen when the phytochemical data are supplemented by ethnobotanical/ethnopharmacological information [33-34]. In the work reported here, it has been shown that the combination of a ligand-based primary *in-silico* screening followed by a protein-based secondary (*in-silico*) screening can provide a reliable means of prospecting natural product databases in the search for new leads in drug discovery. Given that the CHCD search database indirectly embodies ethnopharmacological information, the primary RF screen is both efficient in identifying suitable lead compounds, and sufficiently rapid that it can be used in a truly high throughput manner, permitting desktop processing of thousands of phytochemicals within minutes. The hits so obtained can then be subjected to the more stringent but more time-consuming docking studies, to identify suitable compounds for *in-vitro* testing. By such means, therefore, it will be possible more effectively to exploit the rich resource of plant secondary metabolites in the search for new therapeutic leads.

References

1. Office for National Statistics. Health Statistics Quarterly **1999**, *4*, 59.
2. Elledge**,** R.M.**;** Osborne, C.K. Brit. Med. J. **1997**, *314*, 1843.
3. Brueggemeier, R.W.; Hackett, J.C.; Diaz-Cruz, E.S. Endocrine Rev. **2005**, *26*, 331.
4. Adlercreutz, H. Environ. Health Perspect. **1995**, *103*, 103.
5. Peterson, J.; Lagiou, P.; Samoli, E.; Lagiou, A.; Katsouyanni, K.; La Vecchia, C.; Dwyer, J.; Trichopoulos' D. Br. J. Cancer **2003**, *89***,** 1255.
6. Fink, B.N.; Steck, S.E.; Wolff, M.S.; Britton, J.A.; Kabat, G.C.; Schroeder, J.C.; Teitelbaum, S.L.; Neugut, A.I.; Gammon, M.D. Am. J. Epidemiol. **2006**, *165*, 514.
7. Ehrman, T.M.; Barlow, D.J.; Hylands, P.J. J. Chem. Inf. Mol. Modelling, **2007**, *47*, 254.
8. Hall, L.H.; Kier, L.B. Rev. Comput. Chem. **1991**, *2*, 367.
9. Kier, L.B.; Hall, L.H. *Molecular structure description: the electrotopological state*; Academic Press: London, 1999
10. Labute, P.A. J. Mol. Graphics Modell. **2000**, *18*, 464.
11. Ehrman, T.M.; Barlow, D.J.; Hylands, P.J. J. Chem. Inf. Mol. Model. **2007**, *47*, 264.
12. Ehrman, T.M.; Barlow, D.J.; Hylands, P.J. J. Chem. Inf. Mol. Model. **2007**, *47*, 2316.
13. Berman, H.M.; Westbrook, J.; Feng, Z.; Gilliland, G.; Bhat, T.N.; Weissig, H.; Shindyalov, I.N.; Bourne, P.E. Nucleic Acids Research **2000**, *28*, 235.
14. Favia, A.D.; Cavalli, A.; Masetti, M.; Carotti, A.; Recanatini, M. Proteins – Structure, Function & Bioinformatics **2006**, *62*, 1074.
15. Case, D.A.; Cheatham, T.E.; Darden, T.; Gohlke, H.; Luo, R.; Merz, K.M.; Onufriev, A.; Simmerling, C.; Wang, B.; Woods, R.J. J. Comput. Chem. **2005**, *26*, 1668.
16. Rarey, M.; Kramer, B.; Lengauer, T.; Klebe, G. J. Mol. Biol. **1996**, *261*, 470.
17. Sanderson, J.T.; Hord, I.J.K.; J., Denison, M.S.; Springsteel, M.F.; Nantz, M.H.; van den Berg, M. Toxicol. Sci. **2004**, *82*, 70.
18. Kao, Y.-C.; Zhou, C.; Sherman, M.; Laughton, C.A.; Chen, S. Environ. Health Persp. **1998**, *106*, 85.
19. Aherne,S.A.; O'Brien, N.M. Nutr. Cancer **1999**, *34*, 160.
20. Lee, K.W.; Kang, N.J.; Rogozin, E.A.; Kim, H.-J.; Cho, Y.Y.; Bode, A.M.; Lee, H.J.; Surh, Y.-J.; Bowden, G.T.; Dong, Z. Carcinogenesis **2007**, *28*, 1918.
21. Liu, Z.L.; Tanaka, S.; Horigome, H.; Hirano, T.; Oka, K. Biol. Pharm. Bull. **2002**, *25*, 37.
22. Nomura, T.; Fukai, T.; Akiyama, T. Pure & Appl. Chem. **2002**, *74*, 1199.
23. Fu, B.Q.; Li, H.; Wang, X.R.; Lee, F.S.C.; Cui, S.F. J. Ag. Food Chem. **2005**, *53*, 7408.
24. Pan, X.; Kong, L.D.; Zhang, Y.; Cheng, C.H.K.; Tan, R.X. Acta Pharmacol. Sinica **2000**, *21*, 949.
25. Mounnissamy, V.M.; Gopal, V.; Gunasegaran, R.; Saraswathy, A. Indian J. Heterocyclic Chem. **2002**, *12*, 85.
26. Yoshikawa, M.; Shimada, H.; Shimoda, H.; Murakami, N.; Yamahara, J.; Matsuda, H. Chem. Pharm. Bull. **1996**, *44*, 2086.
27. Graham-Lorence, S.; Khalil, M.W.; Lorence, M.C.; Mendelson, C.R.; Simpson, E.R. J. Biol. Chem. **1991**, *266*,11939.
28. Chen, S.; Kao, Y.C.; Laughton, C.A. J. Steroid Biochem. Mol. Biol. **1997**, *61*, 107.
29. Kao, Y.C.; Cam, L.L.; Laughton, C.A.; Zhou, D.; Chen, S. Cancer Res. **1996**, *56*, 3451.
30. Conley, A.; Mapes, S.; Corbin, C.J.; Greger, D.; Graham, S. Mol. Endocrinol. **2002**, *16*, 1456.
31. Rollinger, J.M.; Langer, T.; Stuppner, H. Planta Medica **2006**, *72*, 671.
32. Rollinger, J.M.; Stuppner, H.; Langer, T. Prog. Drug Res. **2008**, *65*, 213.
33. Rollinger, J.M.; Haupt, S.; Stuppner, H.; Langer, T. J. Chem. Inf. Comput. Sci. **2004**, *44*, 480.

34. Rollinger, J.M.; Hornick, A.; Langer, T.; Stuppner, H.; Prast, H. J. Med. Chem. **2004**, *47*, 6248.

TABLE LEGENDS

Table 1

Phytochemicals with potential aromatase inhibitory activity: their systematic (IUPAC) names, botanical source(s) and Random Forest (RF) activity scores (on a scale of 0.0 – 1.0).

FIGURE LEGENDS

Figure 1

Chemical structures of known aromatase inhibitors: exemastane (A), aminoglutethimide (B), anastrozole (C) and letrosole (D).

Figure 2

Chemical structures of the potential aromatase inhibitors, liquiritigenin (A), gossypetin (B) and myricetin (C).

Figure 3

Molecular model of a potential complex formed between human aromatase and liquiritigenin. Atomic co-ordinates for the enzyme were taken from [12] and the docking of the ligand performed manually using Hyperchem version 7. For the protein residues, covalent geometry is shown using half-bond colouring, according to the colour scheme: carbon, grey; oxygen, red; nitrogen, blue; sulphur, yellow; and hydrogen, white. Liquiritigenin is shown in violet. The molecular solvent accessible surfaces are shown by means of dots, colour-coded according to the underlying atom type (see above). It is notable that the ligand forms no hydrogen bond interactions with the protein but has an L-shaped form that allows it to fit snugly within the available space. Selected residues within the protein active site are labelled.

Figure 4

Molecular model (derived through FlexX docking) of a potential complex formed between human aromatase and gossypetin. Details as for Figure 3. The dihedral angle describing the relative orientation of the (bicyclic) chromene and phenyl rings in the ligand is 60^{o}. Potential hydrogen bonds are shown as dashed lines, and the protein residues involved are labelled.

Figure 5

Aromatase inhibitory activity of (A) liquiritigenin, (B) gossypetin, (C) myricetin and (D) ketaconazole (positive control), as a function of ligand concentration. Error bars show the standard deviations on the data (n = 4, except for ketoconazole where n = 3). Arrows indicate the calculated IC-50s of the inhibitors.

Table 1

Constituent	IUPAC name	Botanical source(s)	RF score
Daidzein	4',7-Dihydroxyisoflavone	*Sophora subprostrata*	0.994
Genistein	4',5,7-Trihydroxyisoflavone	*Sophora subprostrata*	0.990
Galangin	3,5,7-Trihydroxyflavone	*Alpinia officinarum, Alpinia galanga*	0.988
Norwogonin	5,7,8-Trihydroxyflavone	*Scutellaria* spp.	0.985
Eriodictyol	3',4',5,7-Tetrahydroxyflavanone	Many spp.	0.985
Matairesinol	4,4'-Dihydroxy-3,3'-dimethoxylignan-9,9'-olide	*Arctium lappa*	0.980
Helenalin	6-Hydroxy-4-oxo-2,11(13)-pseudoguaiadien-12,8-olide	*Inula helenium*	0.979
Homoeryodictyol	4',5,7-Trihydroxy-3'-methoxyflavanone	*Coriandrum sativum*	0.975
Liquiritigenin	4',7-Dihydroxyflavanone	*Dalbergia odorifera*	0.973
Demethoxycapillarisin	5,7-Dihydroxy-2-(4-hydroxyphenoxy)-4H-1-benzopyran-4-one	*Artemisia capillaris*	0.972
4-Epiisoinuviscolide	4-Hydroxy-9,11(13)-guaiadien-12,8-olide	*Inula helenium*	0.963
Isoliquiritigenin	2',4,4'-Trihydroxychalcone	*Dalbergia odorifera, Astragalus mongholicus*	0.962
Eupahakonin B	1-Hydroxy-8-(4-hydroxy-2-hydroxymethyl-2E-butenoyloxy)-3,10(14),11(13)-guaiatrien-12,6-olide	*Eupatorium chinense* var. *hakonense*	0.959
Dehydrozaluzanin C	3-Oxo-4(15),10(14),11(13)-guaiatrien-12,6-olide	*Saussurea lappa (& Munnozia maronii)*	0.958
Hesperetin	3',5,7-Trihydroxy-4'-methoxyflavone	*Schizonepeta tenuifolia*	0.956
Isolicoflavonol	3,4',5,7-Tetrahydroxy-3'-prenylflavone	*Glycyrrhiza uralensis*	0.952
Corylinal	2-Hydroxy-5-(7-hydroxy-4-oxo-4H-1-benzopyran-3-yl)benzaldehyde	*Psoralea corylifolia*	0.951
2'-Hydroxygenistein	2',4',5,7-Tetrahydroxyisoflavone	*Lablab niger*	0.941
Licodione	1-(2,4-Dihydroxyphenyl)-3-(4-hydroxyphenyl)-1,3-propanedione	*Glycyrrhiza echinata*	0.939
Gossypetin	3,3',4',5,7,8-Hexahydroxyflavone	*Pyrrosia petiolosa*	0.933
Pinocembrin	5,7-Dihydroxyflavanone	*Glycyrrhiza* spp., *Alpinia katsumadai*	0.930
Scutellarein	4',5,6,7-Tetrahydroxyflavone	*Scutellaria* spp..	0.919
2-Hydroxytomentosin-1,5-epoxide	1,5-Epoxy-2-hydroxy-4-oxo-11(13)-xanthen-12,8-olide	*Xanthium strumarium*	0.912
Epiacetylaleuritolic acid	3-Acetoxy-14-taraxeren-28-oic acid	*Phytolacca acinosa*	0.911
2-Hydroxyalantolactone	2-Hydroxy-5,11(13)-eudesmadien-12,8-olide	*Inula helenium*	0.910
Apigenin	4',5,7-Trihydroxyflavone	*Ginkgo biloba, Pogostemon cablin, Coriandrum sativum*	0.910
Acacetin	5,7-Dihydroxy-4'-methoxyflavone	*Ginkgo biloba*	0.910
Melanoxetin	3,3',4',7,8-Pentahydroxyflavone	*Albizzia lebbek*	0.910
Myricetin	3,3',4',5,5',7-Hexahydroxyflavone	*Impatiens balsamina, Biota orientalis*	0.905
Melandrin	5-Hydroxy-N-(4-hydroxybenzoyl) anthranilic acid	*Melandrium firmum*	0.904

Figure 1

(A)

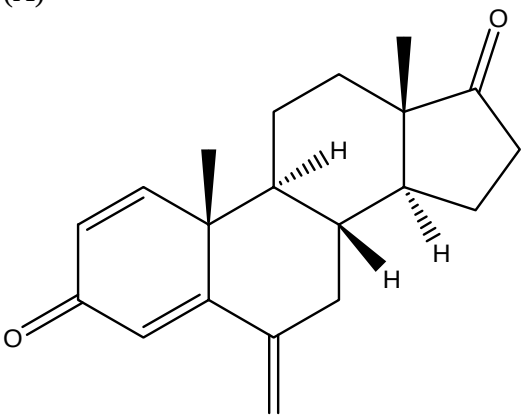

(B)

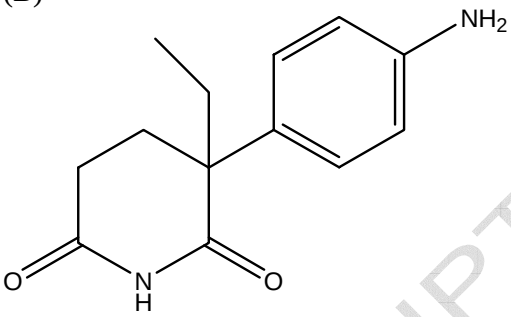

(C)

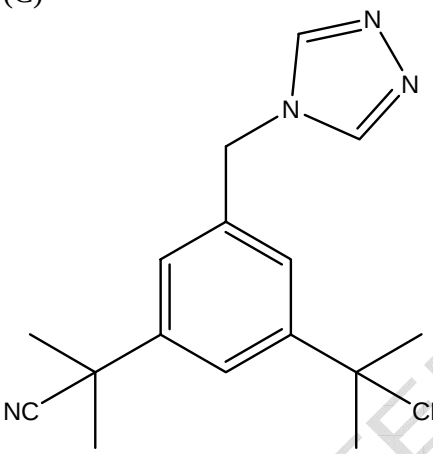

(D)

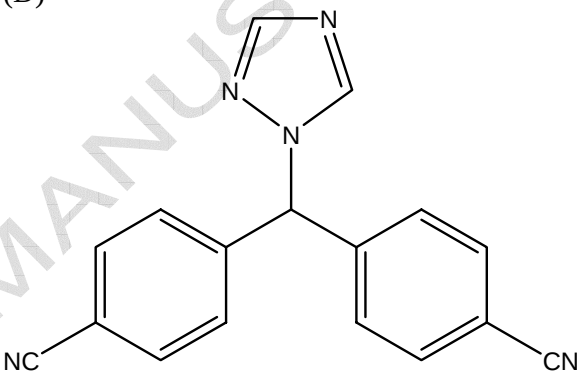

Figure 2

(A)

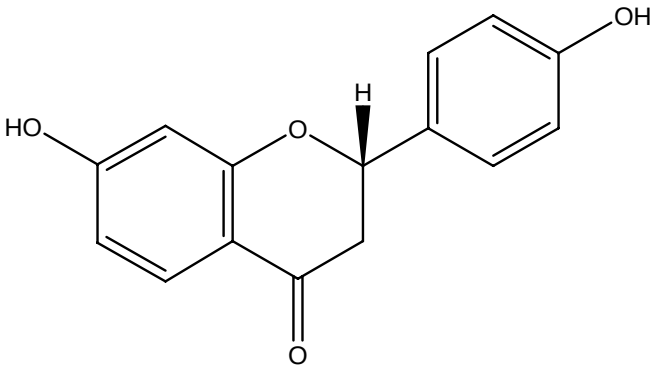

(B)

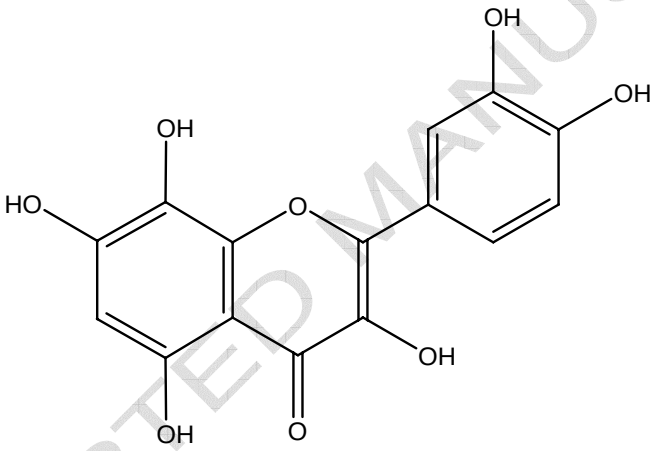

(C)

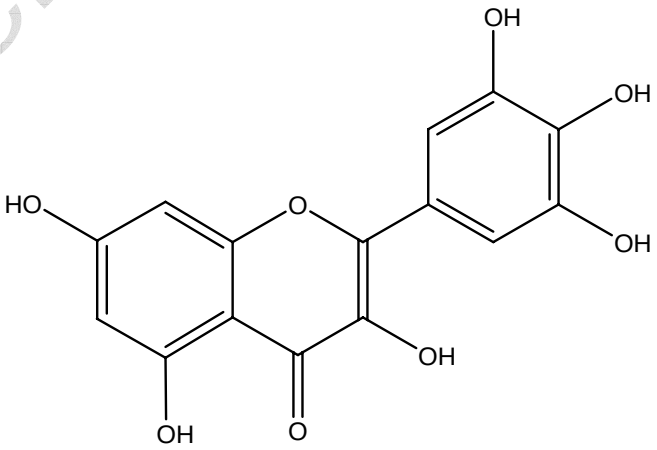

Figure 3

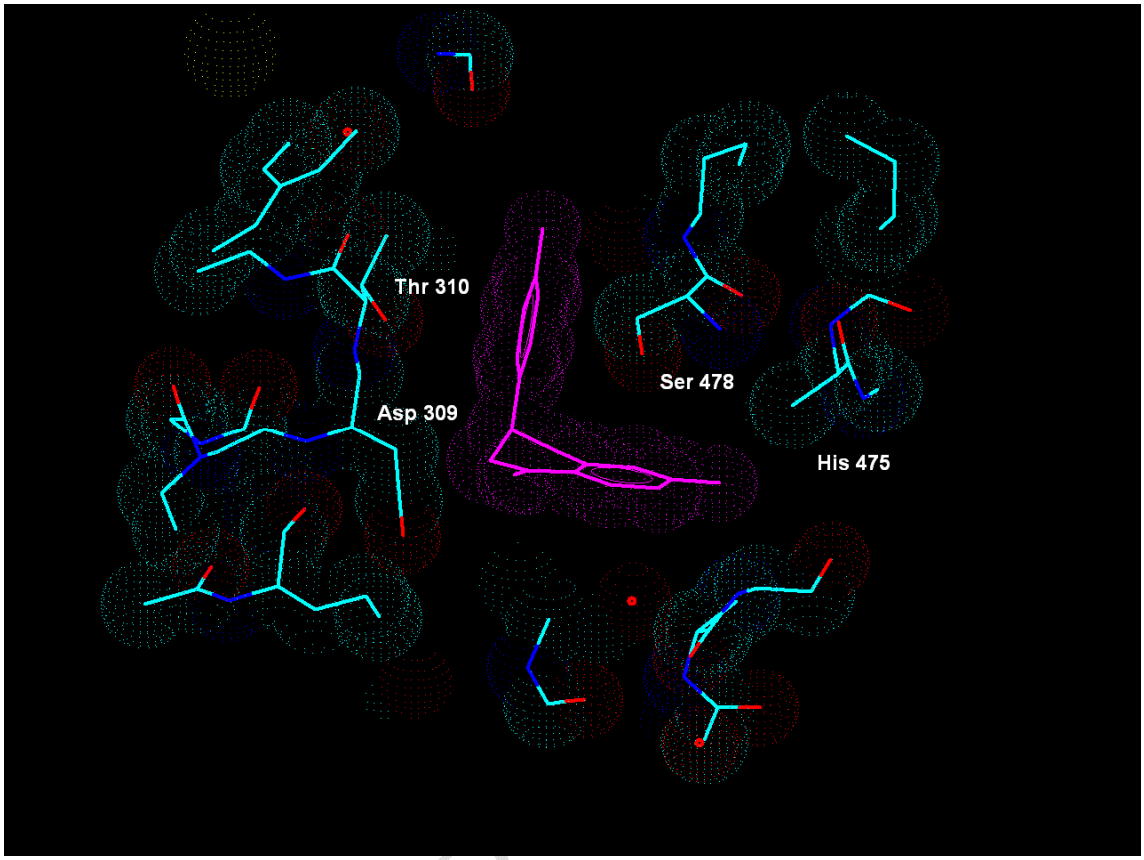

Figure 4

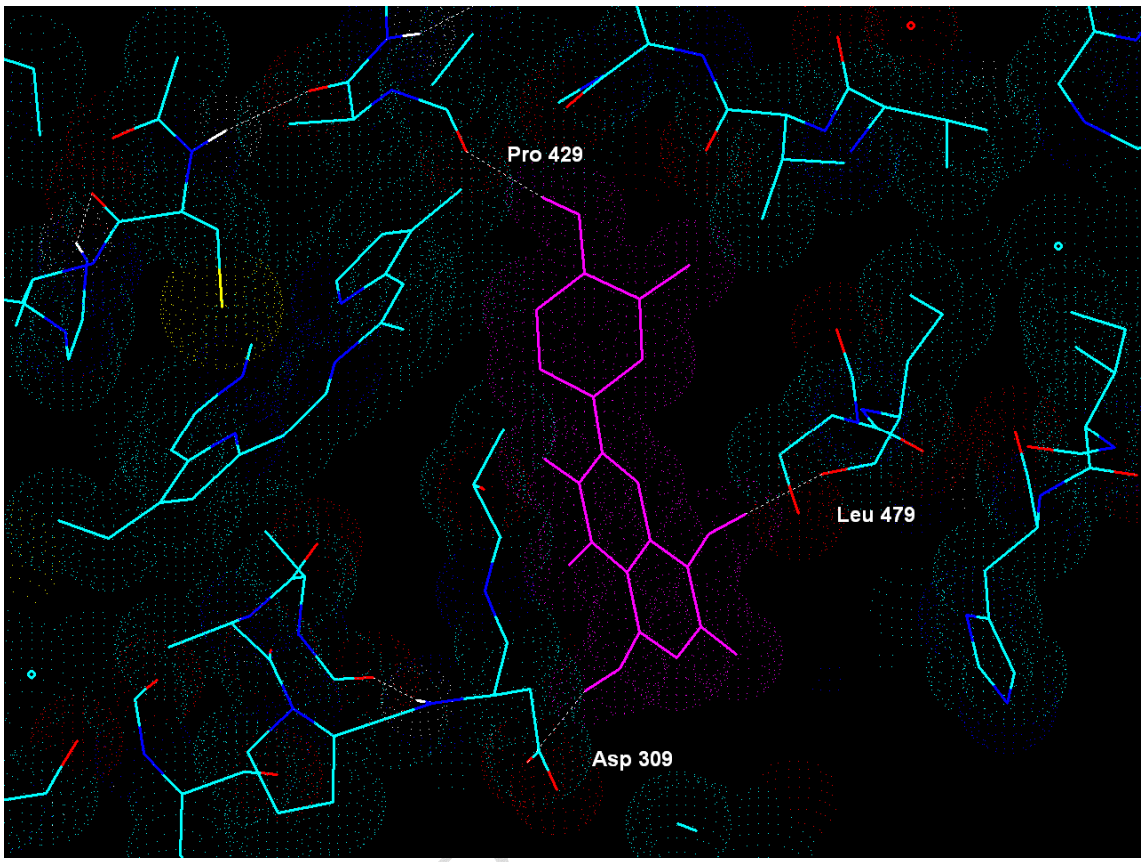

Figure 5

(A)

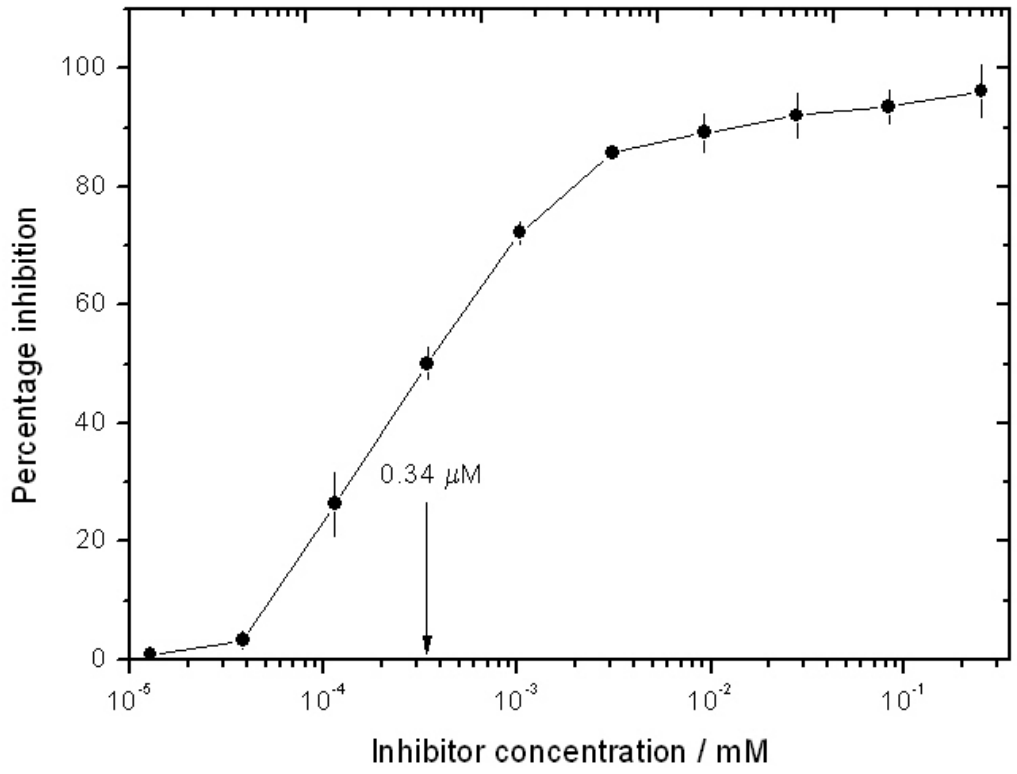

Figure 5

(B)

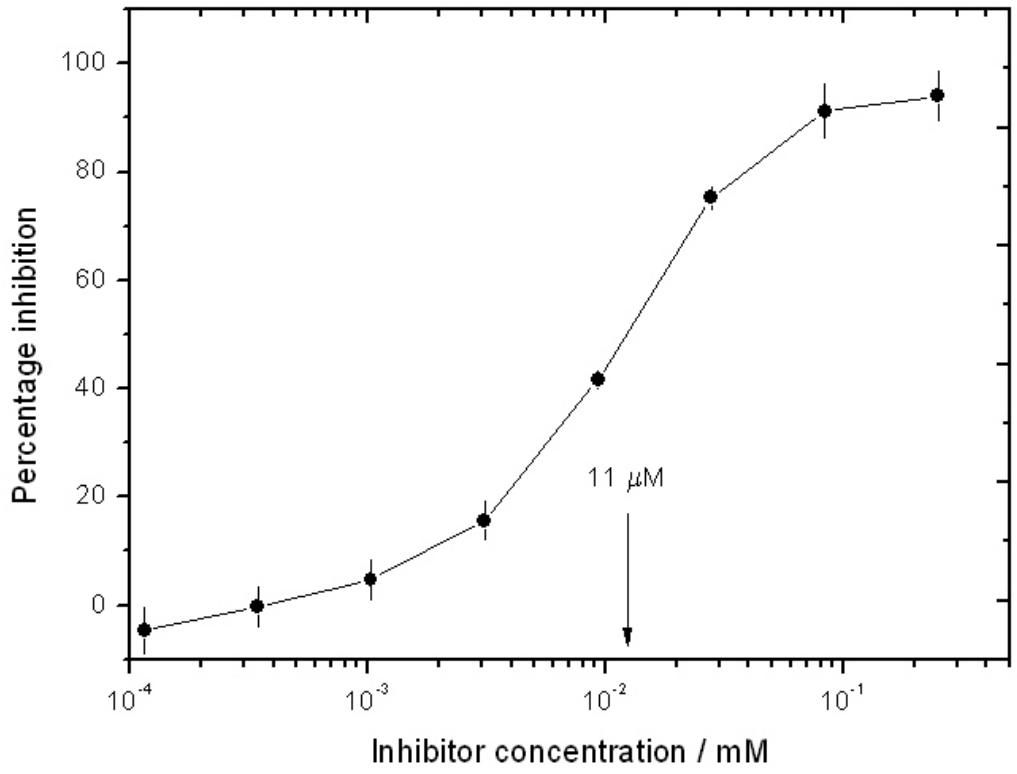

Figure 5

(C)

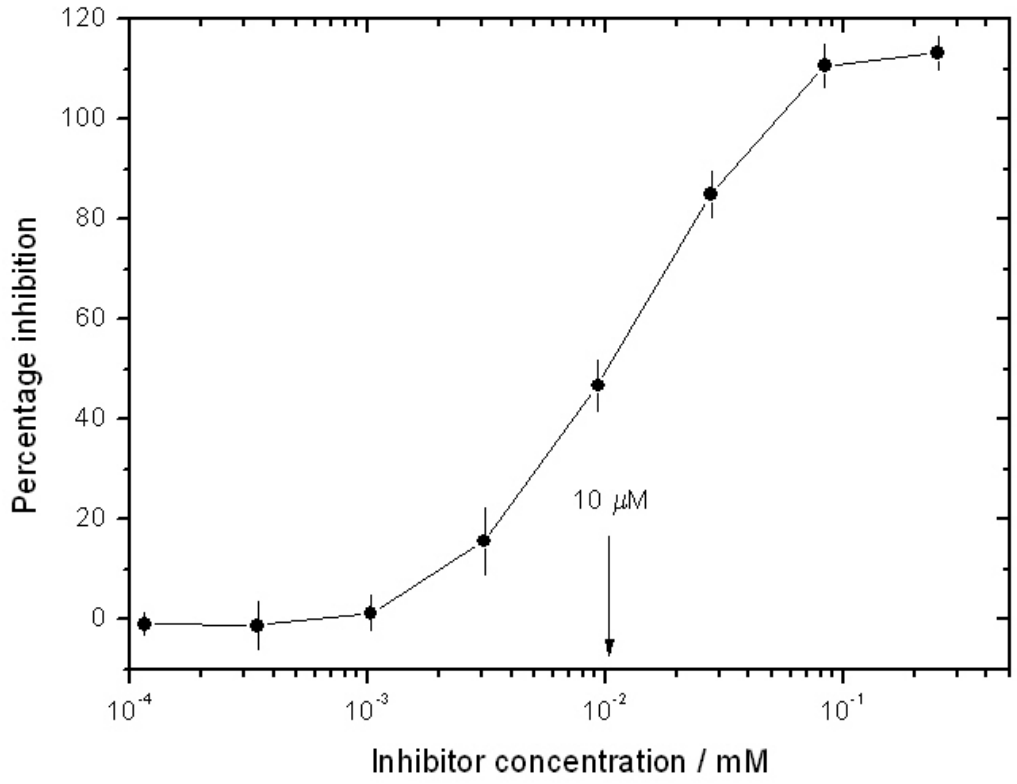

Figure 5

(D)

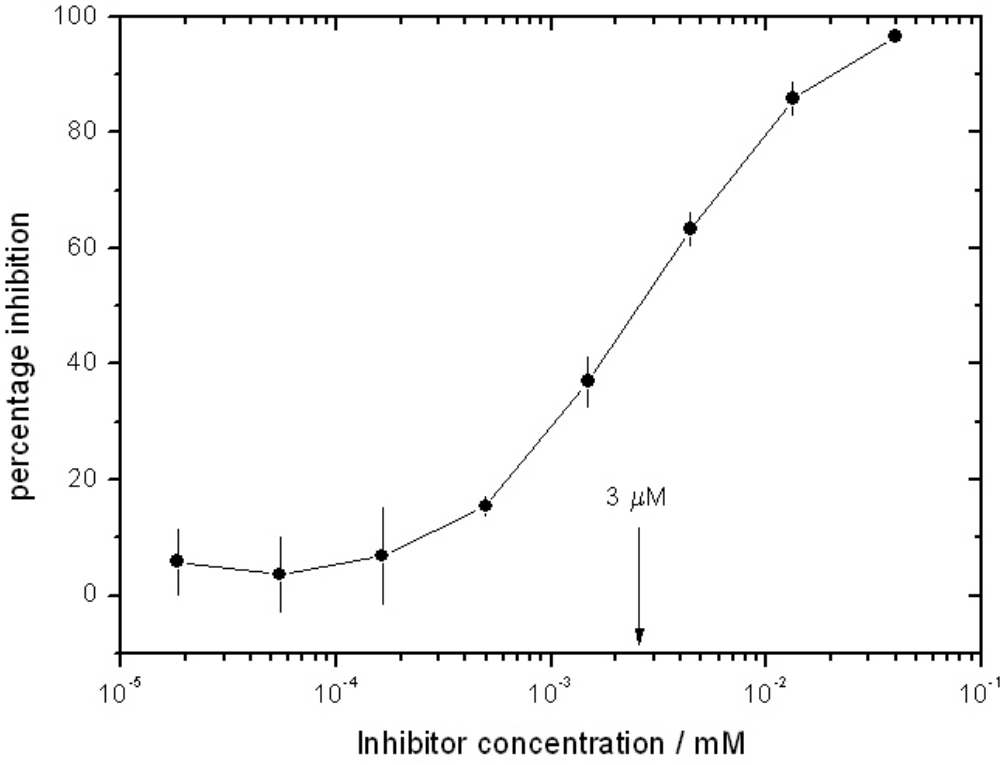

Graphical abstract